doi.org/10.36721/PJPS.2026.39.11.307.1

Prunasin alleviates OGD/R-induced injury in H9c2 cardiomyocytes via SRC/EGFR-AKT-FoxO-mediated mitochondrial quality control

Jiang Li[1#], Yaoshu Li[2#], Chengyang Xu[3*] and Yingying Chen[1]

[1]Henan Provincial Engineering Research Center of Natural Drug Extraction and Medical Technology Application, Zhengzhou Railway Vocational and Technical College, Zhengzhou 450000, China
[2]School of Wushu, Henan University, Kaifeng 475000, China
[3]Department of General Practice Medicine, Henan Provincial People's Hospital, Zhengzhou 450000, China

Abstract: **Background**: Myocardial ischemia-reperfusion injury (MIRI) is still difficult to manage clinically, mainly due to limited effective strategies that can simultaneously address oxidative stress, mitochondrial dysfunction and myocardial cell loss. Prunasin is a cyanide glycoside derived from plants of the genus Prunus. Its biological activity has been reported, but its role in ischemia-reperfusion related cardiac injury is not yet clear. **Objectives**: To evaluate the protective effect of prunasin in an oxygen glucose deprivation/reoxygenation (OGD/R) myocardial cell model and explore its potential mechanism. **Methods**: Firstly, potential targets and pathways were explored through network pharmacology and molecular docking. Then, functional validation was performed using H9c2 cells subjected to OGD/R. Evaluated cell viability, LDH release, apoptosis, ROS levels, ATP content, mitochondrial membrane potential and key signaling proteins. **Results**: Network pharmacology highlighted SRC, EGFR and AKT1 as core targets and molecular docking results showed stable binding between prunasin and SRC, supporting this discovery. In experiments, prunasin increased cell viability in a dose-dependent manner and reduced LDH leakage, cell apoptosis and ROS accumulation. Mitochondrial function is also protected, manifested by the recovery of ATP levels and membrane potential. Mechanistically, prunasin activates the SRC/EGFR-AKT-FxO axis, accompanied by enhanced mitochondrial biogenesis, rebalancing of fission/fusion kinetics and increased mitochondrial autophagy, collectively promoting improved mitochondrial quality control under OGD/R stress conditions. **Conclusions**: Prunasin regulates mitochondrial quality control through the SRC/EGFR-AKT-FxO signaling pathway, thereby reducing OGD/R-induced myocardial cell injury, indicating its potential as a candidate drug for myocardial ischemia-reperfusion intervention.

Keywords: Cardioprotection; Mitochondrial quality control; Prunasin; OGD/R-induced cardiomyocyte injury; SRC/EGFR-AKT-FoxO signaling

Submitted on 19-03-2026 – Revised on 06-05-2026 – Accepted on 25-05-2026

INTRODUCTION

Myocardial cell damage induced by OGD/R is often due to acute coronary occlusion, which interrupts oxygen and glucose supply to the myocardium and triggers a series of ischemic injuries (Huang, Wang *et al*., 2026, Yang, Li *et al*., 2026). Despite improvements in emergency reperfusion and medication interventions, cardiac dysfunction and progression to heart failure after reperfusion remain common and clinically relevant complications (Abate, Nega *et al*., 2023, Cao, Fan *et al*., 2024, Yu, Xu *et al*., 2024). This situation has prompted people to continue exploring more effective heart protection strategies, especially those that can simultaneously target multiple injury mechanisms (Fan, Lin *et al*., 2026, Panossian, 2025). In this context, plant-derived compounds have received increasing attention due to their wide range of biological activities and relatively good safety profiles (Das, Sah *et al*., 2025, Kaur and Kumar, 2025).

Mitochondria are the core determinant of myocardial cell fate during ischemic stress (Mihaylova, Kovacheva *et al*., 2026). In addition to ATP generation, they also integrate redox balance, calcium processing and apoptosis signals (Courmont and Cantelmo, 2026). During ischemia-reperfusion, mitochondrial dynamics disorder and impaired mitochondrial clearance are common phenomena and these changes are closely related to cell death and tissue damage (Jafari and Sahebkar, 2025, Zhao, Cui *et al*., 2025). Therefore, mitochondrial quality control has become an important therapeutic entry point in myocardial protection research (Antoniadou, Shiammoutis *et al*., 2026).

Natural products remain the main source of bioactive molecules with potential cardiovascular benefits (Chen, Gan *et al*., 2025, Wang, Zhu *et al*., 2025). Prunasin is a cyanide glycoside found in several Rosaceae plants such as apricot kernels and bitter almonds (Bhandare and Malode, 2026). It has been reported to have antioxidant and anti-inflammatory activities (Rahaman, Tantra *et al*., 2025). These characteristics suggest that it may have potential roles in diseases driven by oxidative stress and cell apoptosis (Hu, Wu *et al*., 2026, Mia, Hossain *et al*., 2026). However, the role of prunasin in OGD/R-induced myocardial cell injury has not been systematically studied and its potential molecular mechanisms remain unclear (Jin, Zhang *et al*., 2026).

**Corresponding author:* e-mail: xcyhnsy@126.com
#These authors contributed equally and are the co-first authors.

Although reperfusion strategies such as thrombolysis and percutaneous coronary intervention have significantly improved the acute phase prognosis of myocardial infarction, reperfusion related injury remains a persistent challenge. The restoration of blood flow paradoxically induces oxidative stress, inflammatory activation, calcium overload and mitochondrial dysfunction, all of which lead to additional loss of cardiac muscle cells (Chen, Jiang *et al*., 2023, Miranda, 2026). At present, there is still a lack of effective drugs that can specifically target these downstream events, underscoring the need for new mechanism-of-action candidate drugs (Chen, Duffy *et al*., 2026).

In the signal network involved in ischemia-reperfusion injury, the SRC/EGFR-AKT-FoxO axis has attracted significant attention for its role in regulating cell survival, controlling oxidative stress and maintaining mitochondrial function (Hsu, Li *et al*., 2025). Alterations in this pathway can affect the apoptosis threshold and mitochondrial integrity, suggesting its potential relevance in protecting myocardial cells under stress conditions (Muneer, Chen *et al*., 2025). From a methodological perspective, network pharmacology provides a useful framework for exploring the multi-target effects of natural compounds by integrating chemical, genomic and disease databases (Li, Zhang *et al*., 2025, Li and Kar, 2025, Liu, Zhang *et al*., 2024). When combined with pathway enrichment analysis and experimental validation, it can more systematically analyze compound-target interactions and downstream biological effects (Joshi, Baldi *et al*., 2025, Panossian, 2025, Zhao, Zhang *et al*., 2023).

In this study, network pharmacology, molecular docking and in vitro validation were integrated to investigate the protective effects of prunasin against OGD/R-induced myocardial cell injury. Firstly, by calculating and predicting candidate targets and pathways, the SRC/EGFR–AKT–FoxO signaling network and mitochondrial-related processes were selected as the main focus of this study. These predictions were subsequently validated in H9c2 cells subjected to OGD/R. The adoption of this combination strategy aims to move progressively from target prediction to mechanism validation. In summary, the aim of this study is to identify potential molecular targets of prunasin, validate their biological effects in cell injury models and elucidate how they affect signaling pathways related to myocardial cell survival. These results provide mechanistic evidence to support further research on prunasin as a candidate molecule for myocardial ischemia-reperfusion injury.

MATERIALS AND METHODS

Network pharmacology analysis

Active ingredient target prediction

Potential targets of prunasin were predicted using the SwissTargetPrediction database (http://www.swisstargetprediction.ch/; probability > 0.5) and the PharmMapper database (http://www.lilab-ecust.cn/pharmmapper/; matching score > 0.8). The obtained targets were standardized using the UniProt database (https://www.uniprot.org/), with the species restricted to Homo sapiens(Xue, Liu *et al*., 2024).

Disease target collection

Disease-related targets associated with oxygen-glucose deprivation/reperfusion (OGD/R)-induced cardiomyocyte injury and mitochondrial dysfunction were retrieved using the keywords “OGD/R-induced cardiomyocyte injury” and “mitochondrial dysfunction” from multiple publicly available databases, including GeneCards, DisGeNET, OMIM and the Therapeutic Target Database (TTD).

The GeneCards, DisGeNET and OMIM databases were used to retrieve disease-related targets. GeneCards and DisGeNET were applied to obtain gene–disease associations with relevance and confidence scoring, while OMIM was used to complement curated genetic information. The integration of multiple databases was adopted to improve coverage and reliability of target identification. For target screening, a relevance score threshold of >20 was applied for GeneCards and >10 for DisGeNET to ensure high-confidence associations. Targets obtained from different databases were subsequently integrated and duplicate entries were removed based on UniProt identifiers to ensure data consistency and eliminate redundancy.

Construction of protein-protein interaction (PPI) networks

Potential therapeutic targets of prunasin against OGD/R-induced cardiomyocyte injury were identified by intersecting the predicted drug targets with disease-related targets. The overlapping targets were imported into the STRING database (version 11.5; https://string-db.org/) with the species limited to Homo sapiens and the minimum required interaction confidence score set to > 0.7. The resulting PPI network was visualized and analyzed using Cytoscape software (version 3.7.2). Core targets were screened using the CytoHubba plugin based on network topological parameters. Species-mismatched targets were excluded and duplicate targets were merged based on UniProt IDs.

GO and KEGG pathway enrichment analysis

Gene Ontology (GO) functional enrichment analysis and Kyoto Encyclopedia of Genes and Genomes (KEGG) pathway enrichment analysis were performed using the “clusterProfiler” package in R software (version 4.3.1). A p-value < 0.05 and false discovery rate (FDR) < 0.05 were considered statistically significant for enrichment analysis.

Molecular docking

The crystal structure of SRC kinase was retrieved from the RCSB Protein Data Bank. Protein preparation, including removal of water molecules and co-crystallized ligands, addition of polar hydrogens and assignment of Kollman charges, was performed using AutoDock Tools (v1.5.7). The 3D structure of prunasin was obtained from PubChem and energy-minimized prior to docking(Ferreira, Dos Santos *et al*., 2015). Molecular docking was conducted using AutoDock Vina (v1.2.3). The grid box was centered on the ATP-binding pocket of SRC, based on the position of the co-crystallized ligand, with dimensions of 20 × 20 × 20 Å and a spacing of 0.375 Å. The exhaustiveness was set to 8 and 10 binding modes were generated. The docking pose with the lowest binding energy was selected for further analysis. Binding energies below −5.0 kcal/mol were considered indicative of favorable binding affinity. Docking results were visualized using PyMOL (v2.5.0) and Discovery Studio Visualizer (v2021).

In-vitro experimental validation

Cell culture and drug administration

H9c2 cells obtained from the American Type Culture Collection (ATCC; Rockville, MD, USA) were cultured in high-glucose DMEM supplemented with 10% (v/v) fetal bovine serum (FBS), 100 U/mL penicillin and 100 mg/mL streptomycin, in a humidified atmosphere containing 5% CO2 at 37°C. To determine the effects of Prunasin, H9c2 cells were treated with low, medium and high doses (20, 40 and 80 μmol/L) for 24 hours.

H9c2 cells are widely used as an *in-vitro* model for myocardial ischemia-reperfusion injury studies because of their stable growth characteristics, high reproducibility and sensitivity to oxidative and hypoxic stress, making them suitable for mechanistic investigations under controlled experimental conditions. However, since H9c2 cells are derived from embryonic rat ventricular tissue, they cannot fully replicate the electrophysiological and metabolic properties of adult human cardiomyocytes. Therefore, the results of the present study should be interpreted with caution and further validated using primary cardiomyocytes and *in-vivo* models in future studies.

Cell viability assay

The viability of H9c2 cells was assessed using the Cell Counting Kit-8 (CCK-8) assay(Cai, Qin *et al*., 2019). H9c2 cells (1 × 104 cells/well) were seeded into a 96-well plate, supplemented with 100 μl of DMEM and incubated for 24 hours. Subsequently, H9c2 cells were exposed to the culture medium in the presence or absence of prunasin for 24 hours. After treatment, CCK-8 solution (10 μL/well) was added to the culture medium and the culture was further incubated for 2 hours. Finally, the absorbance of the culture medium was measured using a microplate reader (Bio Tek Instruments Inc., Winooski, VT, USA).

Oxygen glucose deprivation/reperfusion (OGD/R)

H9c2 cells were rinsed twice with glucose-free DMEM and the medium was then replaced with glucose-free DMEM supplemented with 10% FBS and 1% penicillin/streptomycin (pre-equilibrated in an anoxic environment at 37°C). Subsequently, the cells were placed in a sealed chamber containing a gas mixture of 5% CO2 and 95% N_2 at 37°C for 6 hours. The oxygen concentration in the hypoxic environment was maintained at <1%, consistent with conditions commonly used in classical cardiomyocyte hypoxia models. Afterward, the cells were refreshed with normal medium and cultured in a humidified atmosphere containing 5% CO2 at 37°C for 24 hours for reperfusion(Zhou, Li *et al*., 2025).

Lactate dehydrogenase (LDH) release assay

The integrity of the cell membrane was assessed using the Lactate Dehydrogenase (LDH) Cytotoxicity Assay Kit (Beyotime, Co., Ltd., C0016, Shanghai, China). Cell culture supernatants from each group were collected and 50 μL of each supernatant was mixed with 50 μL of the reaction working solution in a 96-well plate according to the manufacturer's instructions. The mixture was incubated at room temperature in the dark for 30 minutes. The absorbance was measured at a wavelength of 490 nm using a microplate reader. Cytotoxicity was calculated using the following formula: LDH release rate (%) = (OD value of the experimental group - OD value of the control group) / (OD value of the maximum enzyme activity of the cells - OD value of the control group) × 100%.

Annexin V/PI apoptosis assay

The apoptosis of H9c2 cells was detected using the Annexin V-PI staining kit (Beyotime, Co., Ltd., C1062, Shanghai, China)(Worsley, Veale *et al*., 2022). A total of 1 × 106 cells were collected, washed with PBS and resuspended in 100 μL of binding buffer. Then, 5 μL of Annexin V-FITC and 5 μL of PI staining solution were added, followed by incubation at room temperature in the dark for 15 minutes. After adding 400 μL of binding buffer, the cells were analyzed using a flow cytometer (Beckman Colter CytoFLEX, USA) and the data were analyzed with FlowJo V10 software. The apoptosis rate refers to early apoptosis (Q2 in the flow cytometry dot plot) and late apoptosis (Q3).

TUNEL assay

In situ labeling was performed using the TUNEL Apoptosis Detection Kit (Beyotime, Co., Ltd., C1086, Shanghai, China)(Darzynkiewicz, Galkowski *et al*., 2008). After fixation with 4% paraformaldehyde, cell slides were permeabilized with 0.3% Triton X-100 and incubated with the TUNEL reaction mixture at 37°C for 60 minutes. Following nuclear counterstaining with DAPI, the slides were examined under a fluorescence microscope and the apoptosis rate was calculated as (number of TUNEL-positive cells / total number of cells × 100%).

Mitochondrial function assay

Mitochondrial membrane potential: The mitochondrial membrane potential was detected using the JC-1 fluorescent probe (Beyotime, Co., Ltd., C2006, Shanghai, China)(Sivandzade, Bhalerao *et al*., 2019). After cell treatment, the JC-1 working solution was added and incubated at 37°C for 20 minutes, followed by immediate washing with PBS and detection via fluorescence microscopy (DMI 3000B, Leica, Wetzlar, Germany). The fluorescence intensity was measured using Image J (NIH) to calculate the red/green fluorescence intensity ratio.

Detection of reactive oxygen species (ROS): Intracellular ROS levels were measured using the DCFH-DA fluorescent probe (Beyotime, Co., Ltd., S0033S, Shanghai, China)(Aranda, Sequedo *et al*., 2013). After cell treatment, 10 μM DCFH-DA was added and incubated at 37°C for 20 minutes. The cells were then washed with serum-free medium and immediately subjected to fluorescence microscopy to measure the fluorescence intensity.

ATP content: The intracellular ATP levels were detected using the ATP Content Assay Kit (Beyotime, Co., Ltd., S0026, Shanghai, China, S0026). After cell treatment, the cells were lysed in ATP lysis buffer. The supernatant was collected after centrifugation at 13,000 g for 15 minutes at 4°C and detection was performed at 560 nm. The ATP content was calculated and normalized to the total protein content of the cells.

Western blot

The experimental procedures were performed according to the method described(Kurien and Scofield, 2006).Total cellular proteins were extracted and protein concentration was determined using the BCA method. After SDS-PAGE electrophoresis, membrane transfer and blocking, the primary antibody was added and incubated overnight at 4°C. The secondary antibody was then added and incubated at room temperature for 1 hour, followed by development with ECL chemiluminescent reagent (Yeason Co., Ltd., Shanghai, China). The primary antibodies used in this study were rabbit anti-p-SRC (Tyr 416) (1:1,000, ab278693, Abcam), rabbit anti-SRC (1:1,000, ab109381, Abcam), rabbit anti-p-EGFR (Tyr 1068) (1:1,000, ab40815, Abcam), rabbit anti-EGFR (1:1,000, ab52894, Abcam), mouse anti-p-AKT (Ser 473) (1:2,000, 66444-1-Ig, Proteintech), rabbit anti-AKT (1:2,000, 10176-2-AP, Proteintech), rabbit anti-p-FoxO1 (1:1,000, ab131339, Abcam), rabbit anti-FoxO1 (1:1,000, 18592-1-AP, Proteintech), rabbit anti-p-FoxO3a (Ser 253) (1:2,000, AP0684, ABclonal), FoxO3a (1:2,000, A9270, ABclonal), mouse anti-PGC-1α (1:5,000, 6369-1-Ig, Proteintech), rabbit anti-NRF1 (1:1,000, A3252, ABclonal), rabbit anti-TFAM (1:4,000, A3173, ABclonal), rabbit anti-Drp1 (1:3,000, A21968, ABclonal), rabbit anti-p-Drp1 (Ser616) (1:1,000, AP1573, ABclonal), rabbit anti-p-Drp1(Ser637) (1:1,000, ab193216, Abcam), rabbit anti-Fis1 (1:2,000, 10956-1-AP, Proteintech), rabbit anti-Mfn2 (1:1,000, 12186-1-AP, Proteintech), rabbit anti-OPA1 (1:5,000, 27733-1-AP, Proteintech), rabbit anti-PINK1 (1:1,000, 23274-1-AP, Proteintech), rabbit anti-Parkin (1:500, A0968, ABclonal), mouse anti-LC3B (1:1,000, A17424, ABclonal), mouse anti-SQSTM1/p62 (1:20,000, A19700, ABclonal), rabbit anti-GAPDH (1:50,000, A19056, ABclonal). Quantitative analysis was performed using Image J.

Statistical analysis

Statistical analysis was performed using GraphPad Prism v.10.1. Data distribution was assessed using the Shapiro–Wilk normality test and homogeneity of variance was evaluated using Levene's test. All data were normally distributed and are presented as mean ± standard deviation (SD). Western blot experiments were independently performed three times (n = 3). Band intensities were quantified using ImageJ 1.54c and normalized to GAPDH as the internal control. Statistical comparisons were performed using one-way analysis of variance (ANOVA) followed by Tukey's multiple comparisons post-hoc test for pairwise comparisons among multiple groups. A value of $p < 0.05$ was considered statistically significant.

RESULTS

Network pharmacology analysis

Intersection of prunasin potential targets and OGD/R-induced cardiomyocyte injury disease targets

Using the drug databases PharmMapper and SwissTargetPrediction, 328 and 100 targets were obtained, respectively. After merging and deduplication, a total of 393 potential prunasin targets were identified. Disease-related targets for OGD/R-induced cardiomyocyte injury and mitochondrial dysfunction were obtained from the disease databases GeneCards and OMIM, with 6688 and 408 targets for OGD/R-induced cardiomyocyte injury and 11989 and 395 targets for mitochondrial dysfunction. The intersection of these two diseases yielded 4400 disease-related targets. By intersecting these with the drug targets, 230 common targets were identified, which may represent the potential therapeutic targets for the cardioprotective effects of prunasin (Fig. 1A).

PPI network construction and core target screening

The 230 intersecting targets were uploaded to the STRING database to construct a PPI network comprising 230 nodes and 845 edges (Fig. 1B). The top 10 hub genes were then selected using the MCC (Maximal Clique Centrality) algorithm in the CytoHubba plugin: SRC, EGFR, AKT1, HSP90AA1, GRB2, PIK3R1, JAK2, PTK2, KDR and STAT1 (Fig. 1C).

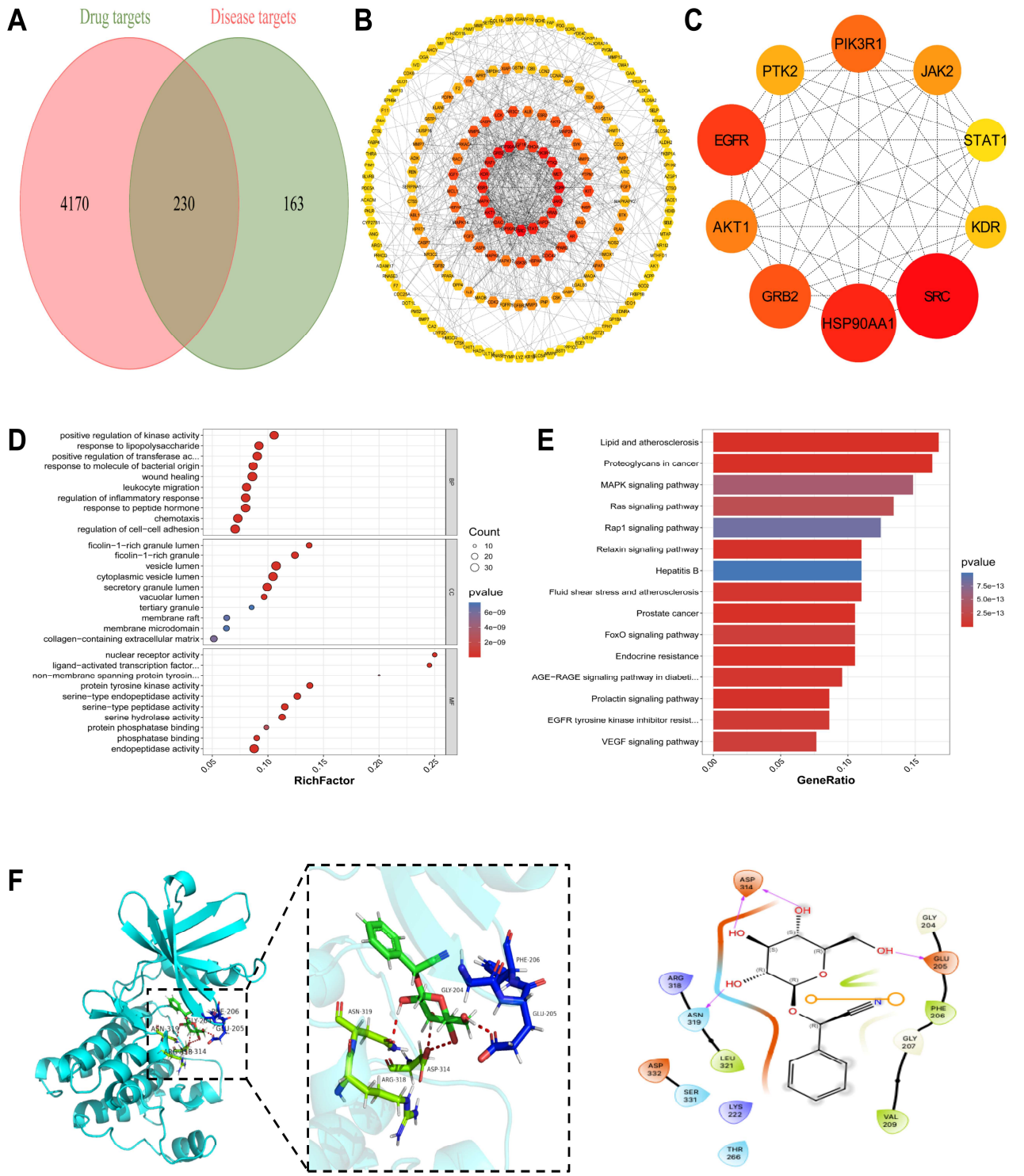

Fig. 1: Network pharmacology analysis of core targets between prunasin and OGD/R-induced injury. (A) Venn diagram of overlapping genes between prunasin and OGD/R-Induced Injury; (B) PPI network visualization; (C) Core gene network map; (D) GO enrichment analysis (BP, CC, MF); (E) KEGG pathways enrichment analysis; (F) Molecular docking map of core targets between prunasin and OGD/R-Induced Injury. GO, gene ontology; KEGG, Kyoto Encyclopedia of Genes and Genomes; PPI, protein–protein interaction.

GO function and KEGG pathway enrichment analysis

GO enrichment analysis revealed that the targets of prunasin are significantly enriched in biological processes such as protein phosphorylation, cellular signal transduction, protein kinase activity and negative regulation of apoptosis; in cellular components including plasma membrane, cytoplasm and mitochondria; and in molecular functions like ATP binding, protein kinase activity and receptor tyrosine kinase activity (Fig. 1D).KEGG pathway enrichment analysis showed that the targets of prunasin are markedly enriched in the PI3K-Akt signaling pathway, EGFR tyrosine kinase inhibitor resistance, FoxO signaling pathway, apoptosis pathway and mitophagy (Fig. 1E).

Molecular docking results

In this study, molecular docking was first performed for SRC, the top-ranked core target in the PPI network. EGFR and AKT1 will be further investigated in subsequent studies. Molecular docking indicated that prunasin exhibits favorable binding affinity toward SRC, with a binding energy of -4.87 kcal mol^{-1}. Prunasin forms hydrogen bonds with key residues ASP 314 and GLU 205 within the SRC active site (Fig. 1F).

In-vitro experimental validation results

The effect of prunasin on the viability of H9c2 cells

To determine the optimal concentration of prunasin for subsequent experiments, its potential cytotoxicity toward H9c2 cells under normal culture conditions was first assessed. (Fig. 2A) and its protective effects in the oxygen-glucose deprivation/reperfusion (OGD/R) injury model (Fig. 2B) using the CCK-8 assay. The corresponding raw absorbance values are presented in table 1 and table 2.

As shown in figure 2A and Table 1, under normal culture conditions, treatment of H9c2 cells with prunasin at concentrations ranging from 1 to 100 μmol/L for 24 hours did not result in significant changes in cell viability compared to the control group (100.0% ± 1.0%) ($p > 0.05$). However, when the concentration was increased to 200 μmol/L, a significant decrease in cell viability was observed (82.6% ± 1.1%; $p < 0.001$), indicating that prunasin exhibits mild cytotoxicity at this concentration.

As shown in Figure 2B and Table 2, in the OGD/R injury model, cell viability in the model group decreased significantly to 53.4% ± 1.0% of that in the control group ($p > 0.05$). Significant protective effects began to appear at 10 μmol/L (59.6% ± 1.9%, $p < 0.001$) and the protective effect gradually increased with increasing concentration. At concentrations of 80 μmol/L and 100 μmol/L, the protective effect reached a plateau, with cell viability recovering to 88.9% ± 1.1% and 90.8% ± 0.9%, respectively ($p < 0.001$ compared to the model group). Notably, at 200 μmol/L, although a significant protective effect was still observed (83.5% ± 1.1%, $p < 0.001$), its efficacy declined slightly compared to that at 100 μmol/L, consistent with its mild toxicity under normal conditions.

Based on the above results, three concentrations—20 μmol/L (with clear and initial protective effects), 40 μmol/L (with significant protective effects) and 80 μmol/L (with near-maximal protective effects and no toxicity) was ultimately selected for further in-depth mechanistic studies, aiming to demonstrate the concentration-dependent effects of prunasin clearly.

The effect of prunasin on LDH release and cell apoptosis

LDH release, flow cytometry and TUNEL staining were used to evaluate cell injury and apoptosis. OGD/R significantly increased LDH leakage compared with the control group, while prunasin reduced LDH release in a dose-dependent manner, with the highest concentration (80 μmol/L) lowering it to 3.6 ± 3.7% (Fig. 3A–B). Annexin V-FITC/PI staining showed an increased apoptotic rate after OGD/R, which was reduced by prunasin treatment (Fig. 3C–D). Consistently, TUNEL staining revealed fewer positive nuclei in prunasin-treated cells (Fig. 3E–F).

The impact of prunasin on mitochondrial function

JC-1 staining showed a decrease in mitochondrial membrane potential after OGD/R in H9c2 cells, which was restored by prunasin in a dose-dependent manner (Fig. 3G and H). DCFH-DA assays showed that intracellular ROS were dramatically elevated after OGD/R (Fig. 3I and J); this increase was concentration-dependently attenuated by prunasin. Furthermore, ATP measurements demonstrated that prunasin reversed the OGD/R-induced decline in cellular ATP content in a dose-dependent manner (Fig. 3K).

Prunasin exerts cardioprotection by activating the SRC/EGFR-AKT-FoxO signaling axis to modulate mitochondrial quality control

To further investigate the mechanism by which prunasin protects cardiomyocytes, the expression levels of key proteins involved in survival signaling pathways and mitochondrial function were assessed by Western blot analysis. The results indicated that prunasin can activate upstream survival signals, thereby coordinately regulating downstream mitochondrial biogenesis, dynamics and autophagy.

Activation of the SRC/EGFR–AKT–FoxO survival signaling pathway by prunasin was first confirmed. Compared with the Ctrl group, OGD/R injury significantly inhibited the phosphorylation activation of upstream signaling molecules, as evidenced by a significant downregulation in the protein levels of p-SRC, p-EGFR and p-AKT ($p < 0.0001$), while the expression levels of the total proteins (SRC, EGFR, AKT) remained unchanged ($p > 0.05$).

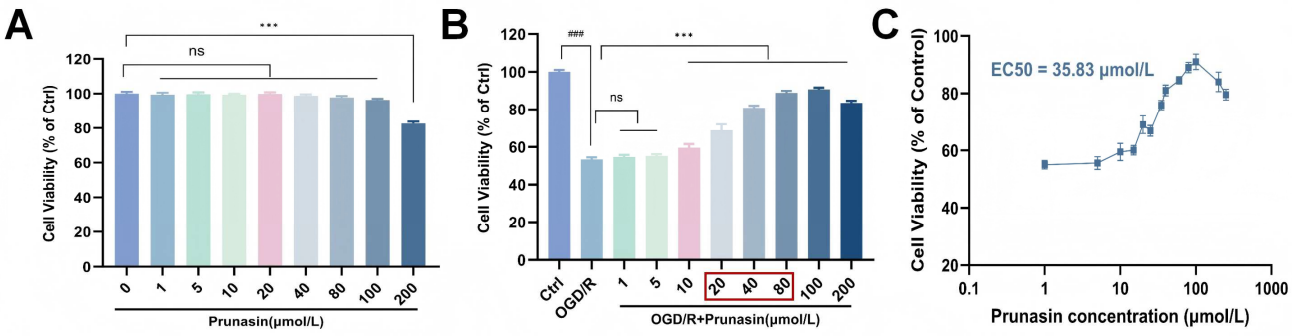

Fig. 2: Determination of prunasin dosage in *in-vitro* experiments. (A) The effect of various concentrations of prunasin on the viability of H9c2 cells was measured using the CCK-8 assay; (B) The effect of various concentrations of prunasin on the recovery of cell viability in H9c2 cells injured by OGD/R was measured using the CCK-8 assay; (C) Dose-response curves (EC50 = 35.83 nM). Data is presented as the mean ± SD (n = 6) of at least three independent experiments. Statistical comparisons were conducted by one-way ANOVA, followed by Tukey's multiple comparisons test. $^{*}p < 0.05$, $^{**}p < 0.01$, $^{***}p < 0.001$ and $^{****}p < 0.0001$ for the indicated comparison; ns, no significant. All experiments were independently repeated three times ($n = 3$).

Table 1: Raw absorbance values for the effect of prunasin on the viability of normal H9c2 cells (toxicity assay).

Prunasin (μmol/L)	Rep1	Rep2	Rep3	Rep4	Rep5	Rep6	Mean ± SD	Viability (% of Ctrl)
Control (0)	1.125	1.134	1.118	1.142	1.109	1.13	1.126 ± 0.012	100.0 ± 1.0
1	1.105	1.128	1.122	1.135	1.104	1.125	1.121 ± 0.011	99.4 ± 1.1
5	1.131	1.12	1.142	1.115	1.109	1.118	1.126 ± 0.011	99.7 ± 1.1
10	1.118	1.107	1.13	1.122	1.115	1.12	1.119 ± 0.008	99.3 ± 0.7
20	1.12	1.132	1.125	1.118	1.14	1.115	1.125 ± 0.010	99.9 ± 0.8
40	1.105	1.118	1.11	1.125	1.1	1.115	1.112 ± 0.009	98.7 ± 0.8
80	1.095	1.11	1.102	1.088	1.115	1.1	1.102 ± 0.010	97.8 ± 0.9
100	1.08	1.095	1.088	1.072	1.09	1.085	1.085 ± 0.009	96.3 ± 0.7
200	0.935	0.92	0.948	0.925	0.915	0.94	0.931 ± 0.013	82.6 ± 1.1***

*Cell viability (%) = ($OD_{treatment\ group}$ / $OD_{control\ group}$) × 100%. Data presented as mean ± SD ($n = 6$). $^{***}p < 0.001$ vs. Vehicle group.

Table 2: Raw absorbance values for H9c2 cell viability following hypoxia/reoxygenation (H/R) injury with prunasin treatment.

Prunasin (μmol/L)	Rep1	Rep2	Rep3	Rep4	Rep5	Rep6	Mean ± SD	Viability (% of Ctrl)
Control	1.125	1.134	1.118	1.142	1.109	1.130	1.126 ± 0.012	100.0 ± 1.0
Model (H/R)	0.605	0.592	0.618	0.588	0.610	0.598	0.602 ± 0.011	53.4 ± 1.0$^{###}$
1	0.615	0.625	0.608	0.632	0.598	0.620	0.616 ± 0.012	54.7 ± 1.1
5	0.615	0.622	0.638	0.630	0.615	0.605	0.621 ± 0.012	55.1 ± 1.0
10	0.645	0.650	0.680	0.675	0.675	0.705	0.672 ± 0.022	59.6 ± 1.9***
20	0.805	0.740	0.818	0.745	0.752	0.802	0.777 ± 0.035	69.0 ± 3.1***
40	0.915	0.900	0.928	0.905	0.892	0.922	0.910 ± 0.014	80.8 ± 1.2***
80	1.005	0.990	1.018	0.995	0.985	1.012	1.001 ± 0.013	88.9 ± 1.1***
100	1.020	1.035	1.008	1.025	1.015	1.030	1.022 ± 0.010	90.8 ± 0.9***
200	0.945	0.930	0.958	0.935	0.925	0.950	0.941 ± 0.013	83.5 ± 1.1***

*Cell viability (%) = (OD $_{treatment\ group}$ / OD $_{control\ group}$) × 100%. Data are presented as mean ± SD ($n = 6$). $^{###}p < 0.001$ vs. control group; $^{***}p < 0.001$ vs. model (H/R) group.

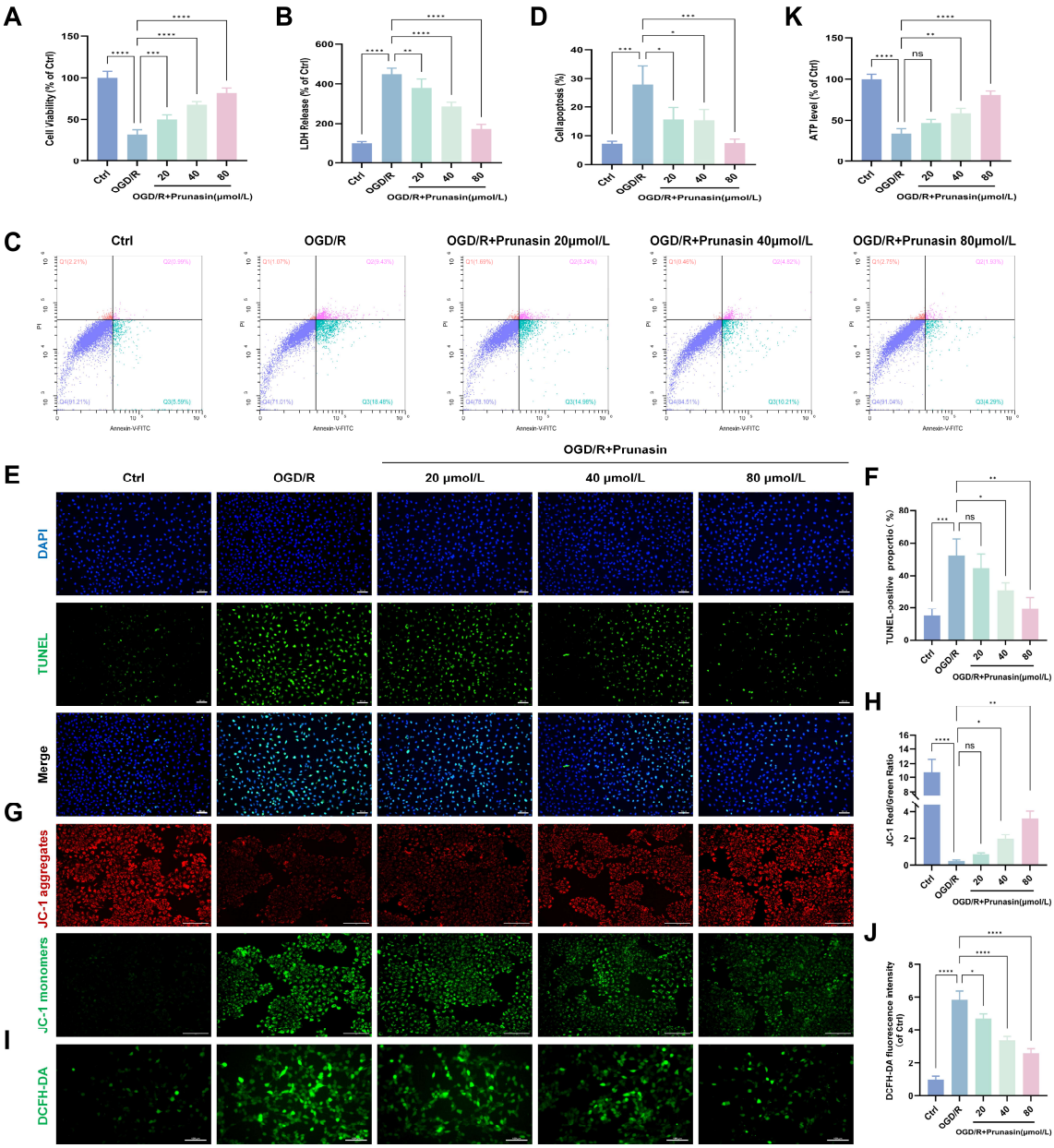

Fig. 3: Prunasin alleviates the effects of OGD/R on H9c2 cells. (A) The effect of various concentrations of prunasin on the recovery of cell viability in H9c2 cells injured by OGD/R was measured using the CCK-8 assay; (B) LDH release in the medium of H9c2 cells; (C) Flow cytometry analysis for H9c2 cell apoptosis after Annexin V/PI staining; (D) Quantitative analysis of the apoptotic H9c2 cell. (E) TUNEL staining was used to detect apoptosis in H9c2 cells. Cell nuclei were counterstained with DAPI (blue); (F) Quantitative assessment of the proportion of apoptotic cells in the TUNEL assay. 10 × magnification; Scale bar, 100 μm; (G) Representative images of H9c2 cells stained with JC-1 for visualization of mitochondrial membrane potential. Aggregates were stained red, and monomers were stained green. 10 × magnification; Scale bar, 100 μm; (H) Analysis of the ratio of red/green fluorescent density; (I) Staining of intracellular ROS by DCFH-DA staining in H9c2 cells. 10 × magnification; Scale bar, 100 μm; (J) DCFH-DA fluorescence intensity in H9c2 cells relative to the ctrl group; (K) ATP content relative to the ctrl group. OGD/R, oxygen-glucose deprivation/reperfusion; LDH, lactate dehydrogenase; ROS, reactive oxygen species; DHE, dihydroethidium; DCFH-DA, 2',7'-dichlorodihydrofluorescein diacetate; ATP, adenosine triphosphate. Data are presented as the mean ± SD (n = 6) of at least three independent experiments. Statistical comparisons were conducted by one-way ANOVA, followed by Tukey's multiple comparisons test. $^{*}p < 0.05$, $^{**}p < 0.01$, $^{***}p < 0.001$, and $^{****}p < 0.0001$ for the indicated comparison; ns, no significant. All experiments were independently repeated three times (n = 3).

Prunasin treatment concentration-dependently reversed this suppression, as evidenced by significantly increased phosphorylation levels of SRC, EGFR and AKT. Consequently, the phosphorylation of the downstream transcription factor FoxO3a at Ser253 was also elevated. These data suggest that the SRC/EGFR-AKT pathway is activated by prunasin, leading to increased inhibitory phosphorylation of FoxO3a (Figs. 4A-B).

Subsequently, the mitochondrial biogenesis process downstream of FoxO signaling was investigated. OGD/R injury significantly reduced the protein expression of the "master switch" of mitochondrial biogenesis, PGC-1α and its downstream effector, TFAM ($p < 0.0001$). After intervention with prunasin, the expression of these proteins was restored in a concentration-dependent manner. This result is consistent with the aforementioned conclusion that FoxO is inhibited, suggesting that prunasin may restore mitochondrial biogenesis by relieving FoxO-mediated transcriptional repression of PGC-1α (Figs. 4C-D).

Next, changes in mitochondrial dynamics balance were evaluated. OGD/R injury disrupted the balance between mitochondrial fission and fusion, characterized by a significant upregulation in the expression of the fission - promoting protein Drp1 and its activated form p - Drp1 (Ser616), while the expression of its inhibitory form p - Drp1 (Ser637) and the fusion - promoting protein Mfn2 was significantly downregulated ($p < 0.001$). Prunasin treatment effectively corrected this imbalance, inhibiting fission and promoting fusion in a concentration-dependent manner, thereby helping maintain mitochondrial network integrity (Figs. 4E-F).

Finally, changes in mitophagic flux were examined. After OGD/R injury, the expression of autophagy - initiating proteins PINK1, Parkin and LC3B-II was significantly increased ($p < 0.0001$), while the autophagy substrate p62 was extensively accumulated ($p < 0.01$), indicating that although autophagy was initiated, the degradation process was severely impaired. Prunasin increased the expression of PINK1 and Parkin, while reducing p62 protein levels ($p < 0.0001$). LC3B-II levels were also elevated following treatment. These changes suggest an enhancement of mitophagy activity and improved clearance of damaged mitochondria (Figs. 4G–H).

DISCUSSION

This study combines network pharmacology and *in vitro validation to demonstrate that prunasin alleviate OGD/R-induced damage in cardiomyocytes, at least partially by regulating the SRC/EGFR-AKT-FxO signaling axis and mitochondrial mass regulation*. These results support that prunasin, as a multi-target natural compound, may help maintain mitochondrial homeostasis - a key determinant of myocardial cell survival under ischemia-reperfusion stress.

Despite continuous progress in reperfusion strategies, including thrombolysis and percutaneous coronary intervention, myocardial ischemia-reperfusion injury (MIRI) remains a significant clinical issue. Although reperfusion can restore coronary artery blood flow, it is also accompanied by oxidative stress, inflammatory activation, calcium overload, mitochondrial dysfunction and myocardial cell loss. At present, the selection of drugs that can effectively intervene in these interrelated processes remains limited, underscoring the need for multi-target therapy strategies.

In this context, the SRC/EGFR-AKT-FoxO signaling axis is increasingly recognized as an important regulatory node in cell survival and stress adaptation. The activation of SRC and EGFR can converge on the AKT signaling pathway, thereby regulating FoxO transcription factors through phosphorylation-dependent inactivation. This study found that prunasin can affect this signaling cascade, which may be one of the mechanisms by which they alleviate stress signals and improve mitochondrial function under OGD/R conditions.

Network pharmacology analysis identified SRC, EGFR and AKT1 as the core nodes in the predicted target network. Enrichment analysis further highlighted pathways related to PI3K/Akt and FoxO signaling, consistent with experimental observations. Molecular docking suggests that wild cherry glycoside may interact with SRC, but the binding affinity needs further experimental verification.

At the downstream level, changes in FoxO-related signals are accompanied by alterations in mitochondrial biomarkers. After treatment with prunasin, recovery of PGC-1α and TFAM was observed, consistent with reduced transcriptional inhibition by FoxO and with previous research linking FoxO activity to mitochondrial biogenesis regulation.

Functionally, prunasin increased the cell viability of H9c2 cells damaged by OGD/R, reduced LDH release, cell apoptosis and ROS accumulation. These effects are accompanied by the recovery of ATP levels and mitochondrial membrane potential, indicating an improvement in mitochondrial function. Consistently, prunasin regulate phosphorylation levels in the SRC/EGFR-AKT pathway and alter downstream proteins involved in mitochondrial biogenesis, dynamics and autophagy.

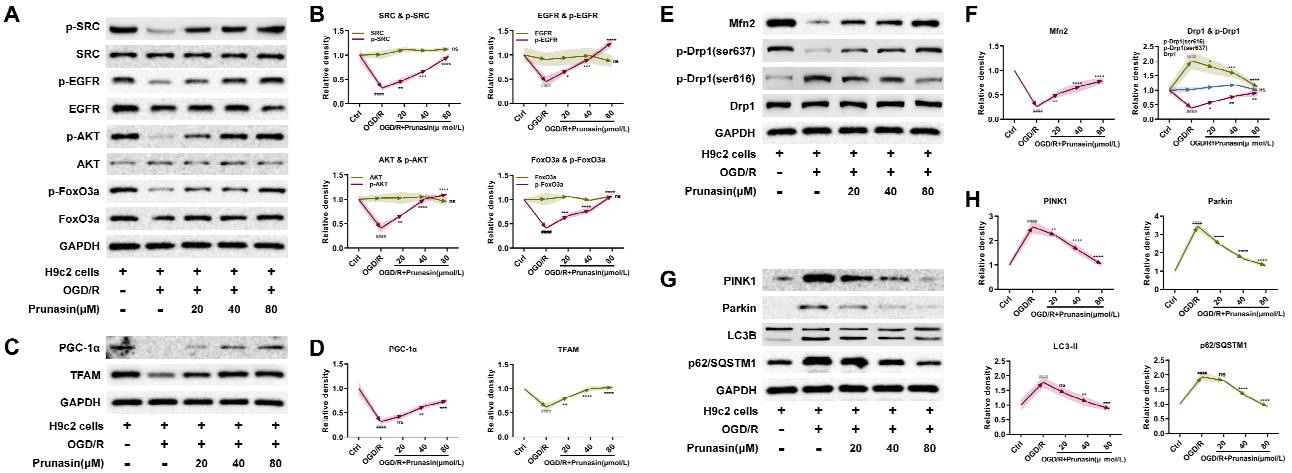

Fig. 4: *In-vitro* experiments validated that activating the SRC/EGFR-AKT-FoxO signaling axis regulates mitochondrial quality control to exert cardioprotective effects. The levels of proteins related to the upstream survival signals (A-B), mitochondrial biogenesis downstream of FoxO signaling; (C-D) mitochondrial dynamics balance; (E-F) and mitochondrial autophagy flux; (G-H) in H9c2 cells were detected by Western blot, followed by quantitative analysis. Data are presented as the mean ± SD (n = 3) of at least three independent experiments. Statistical comparisons were conducted by one-way ANOVA, followed by Tukey's multiple comparisons test. $^{\#\#\#\#}p < 0.0001$ vs. Ctrl, $^{*}p < 0.05$, $^{**}p < 0.01$, $^{***}p < 0.001$ and $^{****}p < 0.0001$ vs. OGD/R; ns, no significant. All experiments were independently repeated three times (n = 3).

Mitochondrial quality control closely depends on the balance between division and fusion. Drp1 mediated excessive fission leads to mitochondrial fragmentation and ROS production, while Mfn2 mediated fusion supports mitochondrial integrity and metabolic stability. In this study, OGD/R disrupted this balance, while prunasin partially restored it by inhibiting Drp1 and increasing Mfn2 expression. This transformation is accompanied by reduced oxidative stress and improved mitochondrial function. The changes in mitochondrial autophagy-related proteins further suggest enhanced clearance of damaged mitochondria, which may help cells adapt to stress conditions.

Overall, the data indicates that prunasin exert their protective effects by coordinating the regulation of survival signals and mitochondrial quality control. However, these findings are preliminary and based on in *vitro* models, so they should be interpreted accordingly.

Several limitations need to be considered. Prunasin is a cyanide glycoside and its in vivo safety, especially regarding potential cyanide release and metabolic conversion issues, still needs to be clarified. The current safety evaluation is limited to *in-vitro* conditions and may not reflect systemic exposure. Furthermore, although network pharmacology identifies putative targets, these targets require functional validation through genetic or pharmacological interventions. Finally, the use of H9c2 cells cannot fully reproduce the complex inflammatory, neurohumoral and hemodynamic environment of myocardial ischemia-reperfusion injury *in-vivo*. Future research should use animal models, combined with pharmacokinetic analysis and metabolite identification, to more comprehensively evaluate their translational potential.

CONCLUSION

This study used a combination of network pharmacology, molecular docking and *in-vitro* validation to investigate the protective effect of prunasin on H9c2 myocardial cell injury induced by oxygen-glucose deprivation/reoxygenation (OGD/R). The results showed that prunasin can alleviate cell damage caused by OGD/R, as evidenced by increased cell viability, reduced lactate dehydrogenase (LDH) release and partial restoration of mitochondrial function. In terms of mechanism, integrated analysis identified SRC, EGFR and AKT1 as potential targets of prunasin. The experimental data further suggest that prunasin may regulate the SRC/EGFR-AKT-FxO signaling pathway, which may explain its improvement in mitochondrial quality control under stress conditions. In summary, these findings suggest that prunasin may exert cardioprotective effects by supporting mitochondrial homeostasis during OGD/R injury. This study provides preliminary evidence of its potential biological relevance and lays the foundation for future mechanistic and in vivo research on myocardial ischemia-reperfusion injury.

Acknowledgments
The authors would like to thank all members of the

research team for their valuable assistance and constructive discussions during this study.

Authors' contributions

J. L. and Y. L: Conceived and designed the study; J. L., Y. L. and Y. C: Performed the experiments; C. X: Provided technical assistance and guidance for the OGD/R model establishment and molecular mechanism investigations; J. L. and Y. L: Conducted data analysis and interpretation. All authors contributed to drafting and revising the manuscript. All authors have read and approved the final version of the manuscript and agree to be accountable for all aspects of the work.

Funding

This work was supported by the Key Projects Jointly Constructed by Henan Province and Ministry of Medical Science and Technology Research Plan (No. SBGJ202102030), the Scientific and technological research projects of Henan province (No. 242102310370), the Major Science research Project of high Education of Henan Province (No. 26B310014) and the Science research Project of Zhengzhou Railway Vocational and Technical College (No. 2025KY011).

Data availability statement

The datasets generated during and/or analysed during the current study are available from the corresponding author on reasonable request.

Ethical approval

This study did not involve human participants, human-derived samples, clinical specimens, identifiable personal data, or animal experiments. All experiments used commercially available H9c2 cells (Stemrecell, China; Item No. STM-CL-7921) and standard laboratory reagents.

Conflict of interest

The authors declare that there are no conflicts of interest regarding the publication of this paper.

REFERENCES

Abate SM, Nega S, Basu B and Bekele T (2023). Global burden of postoperative Myocardial infarction among noncardiac surgical patients: A systematic review, meta-analysis and meta-regression. *Trends Anaesth Crit Care,* **50** 101252.

Antoniadou K, Shiammoutis I and Piperi C (2026). Therapeutic impact of mitochondrial transplants for cardiovascular diseases. *Int J Mol Sci.,* **27**(9) 4018.

Aranda A, Sequedo L, Tolosa L, Quintas G, Burello E, Castell J and Gombau L (2013). Dichloro-dihydro-fluorescein diacetate (DCFH-DA) assay: A quantitative method for oxidative stress assessment of nanoparticle-treated cells. *Toxicolo in vitro.,* **27**(2) 954-963.

Bhandare SD and Malode SS (2026). Toxic plant metabolites, cyanogenic glycosides, poisoning mechanisms, health risks and analytical method development for detecting toxicants in food. *Food Drug Saf* **3**(1) 114-146.

Cai L, Qin X, Xu Z, Song Y, Jiang H, Wu Y, Ruan H. Chen J (2019). Comparison of cytotoxicity evaluation of anticancer drugs between real-time cell analysis and CCK-8 method. *ACS Omega* **4**(7) 12036-12042.

Cao Y, Fan R, Zhu K. Gao Y (2024). Advances in functionalized hydrogels in the treatment of myocardial infarction and drug-delivery strategies. *ACS Appl MaterInterfaces,* **16**(37): 48880-48894.

Chen G, Gan J, Wu F, Zhou Z, Duan Z, Zhang K, Wang S, Jin H, Li Y and Zhang C (2025). Scpep1 inhibition attenuates myocardial infarction-induced dysfunction by improving mitochondrial bioenergetics. *EurHeart J* **46**(26): 2579-2594.

Chen G, Jiang N, Zheng J, Hu H, Yang H, Lin A, Hu B, and Liu H (2023). Structural characterization and anti-inflammatory activity of polysaccharides from Astragalus membranaceus. *Int J Biol Macromol.,* **241**: 124386.

Chen R, Duffy Á, and Do R (2026). Genomics of drug target prioritization for complex diseases. *NatRev Genet,* **27**(3): 231-245.

Courmont E and Cantelmo AR (2026). Calcium signaling and metabolic reprogramming in cancer: Mechanisms and therapeutic implications. *Cold Spring Harb Perspect Biol,* **18**(4): a041764.

Darzynkiewicz Z, Galkowski D and Zhao H (2008). Analysis of apoptosis by cytometry using TUNEL assay. *Methods,* **44**(3): 250-254.

Das J, Sah AK, Choudhary RK, Elshaikh RH, Bhui U, Chowdhury S, Abbas AM, Shalabi MG, Siddique NA and Alshammari RR (2025). Network pharmacology approaches to myocardial infarction reperfusion injury: Exploring mechanisms, pathophysiology and novel therapies. *Biomedicines,* **13**(7): 1532.

Fan Y, Lin L, Huang K, Lin J, Xu J, Zhou X. Yang Y (2026). Interleukin 33 regulates the autophagy of oxygen-glucose-deprivation/reoxygenation microglia via macrophage polarization. *Cent Eur J Immunol*. **51**(1):84-94

Ferreira LG, Dos Santos RN, Oliva G. Andricopulo AD (2015). Molecular docking and structure-based drug design strategies. *Molecules,* **20**(7): 13384-13421.

Hsu CH, Li YJ, Guo TN, Tzou FY, Hong CL, Lin CH, Huang SY and Chan CC (2025). The cell autonomous and non-autonomous functions of Rab27 in longevity and neuroprotection in Drosophila. *Autophagy,* **21**(12): 2809-2825.

Hu X, Wu Y, Chen Q, Chen Z and Li Q (2026). Insights into the cell type-specific susceptibility of kidney cells to ferroptosis. *Drug Discov Today,* 104598.

Huang X, Wang S, Xue T, Wang Y, Yan Q, Zhu X, Li H, Chen F, Zhang Y and Cui X (2026). CD44 alleviates

myocardial ischemia reperfusion injury through repressing ferroptosis. *Int Immunopharmacol.,* **172**: 116230.

Jafari A and Sahebkar A (2025). Can ginger improve cardiovascular health indices? A protocol for a GRADE-assessed systematic review and planned dose–response meta-analysis of randomized controlled trials. *Syst rev* **14**(1): 121.

Jin B, Zhang Y, Lin J, Zhu Y, Yang M, Zhang Y, Yin Y, Zhang Z, Yang M and Jiang J (2026). Dihydromyricetin confers protection against myocardial ischemia-reperfusion injury by inhibiting ferroptosis through direct targeting of PPARα. *Front Pharmacol,* **17**: 1794756.

Joshi CP, Baldi A, Kumar N and Pradhan J (2025). Harnessing network pharmacology in drug discovery: An integrated approach. *Naunyn-Schmiedeberg's Arch Pharmacol.,* **398**(5): 4689-4703.

Kaur A and Kumar R (2025). Use of herbal drugs in cardiovascular disease-A review. *Curr Cardiol Rev.,* **21**(1): E1573403X1323724.

Kurien BT and Scofield RH (2006). Western blotting. *Methods,* **38**(4) 283-293.

Li D, Zhang P and Chen H (2025). Advanced therapeutic strategies in digestive and circulatory health: nanomedicine and beyond, *Front Med SA*. 1666774.

Li L and Kar S (2025). Leveraging network pharmacology for drug discovery: Integrative approaches and emerging insights. *Med Drug Discov* 100220.

Liu Q, Zhang D, Wang B, Zhao W, Zhang T, Sutcharitchan C and Li S (2024). Network pharmacology: Advancing the application of large language models in traditional Chinese medicine research. *Sci Tradit Chin Med.,* **10**:1097.

Mia E, Hossain MA, Alshahrani MY, Shipon MNH, Rakib IH, Bhuia MS, Uddin MB, Islam MT and Al Hasan MS (2026). Targeting cancer through oxidative stress: The role of epigallocatechin gallate in reactive oxygen species modulation. *J Biochem Mol Toxicol.,* **40**(2): e70697.

Mihaylova V, Kovacheva E, Gevezova M, Sarafian V and Kazakova M (2026). Mitochondria as an integrative hub of cellular homeostasis and stress response. *Int J Mol Sci.,* **27**(9): 3871.

Miranda CH (2026). Longitudinal assessment of endothelial glycocalyx in ST-elevation myocardial infarction: Interplay with oxidative stress and inflammation. *Microvasc Res.,* 104926.

Muneer G, Chen CS and Chen YJ (2025). Advancements in global phosphoproteomics profiling: Overcoming challenges in sensitivity and quantification. *Proteomics* **25**(1-2): e202400087.

Panossian A (2025). Trends and pitfalls in the progress of network pharmacology research on natural products. *Pharmaceuticals,* **18**(4): 538.

Rahaman TA, Tantra T and Chaudhary S (2025). Natural-product-inspired potent anticancer congeners: chronological advancements, structure-activity relationship (SAR) studies and future perspectives. *Bioorg & Med Chem,* 118392.

Sivandzade F, Bhalerao A and Cucullo L (2019). Analysis of the mitochondrial membrane potential using the cationic JC-1 dye as a sensitive fluorescent probe. *Bio-proto,* **9**(1): e3128-e3128.

Wang C, Zhu F, Zhou L, Zhang S, Wang R, Tian H, Zhang B, Wu J, Xu X and Jiang R (2025). Krüppel like factor 7 regulates mitochondrial dynamics balance in myocardial infarction. *Commun Biol.,* **8**(1): 722.

Worsley CM, Veale RB. Mayne ES (2022). Inducing apoptosis using chemical treatment and acidic pH and detecting it using the Annexin V flow cytometric assay. *Plos One,* **17**(6): e0270599.

Xue QQ, Liu CH and Li Y (2024). Decoding the anti-hypertensive mechanism of α-mangostin based on network pharmacology, molecular docking and experimental validation. *Mol Med.,* **30**(1): 234.

Yang Y, Li C, Lu Z, Cao X and Wu Q (2026). Synergistic effects of CAR-modified mesenchymal stem cells and MGST1 activation in facilitating myocardial tissue repair post-ischemia-reperfusion injury. *Arch Biochem Biophys,* 110798.

Yu T, Xu Q, Chen X, Deng X, Chen N, Kou MT, Huang Y, Guo J, Xiao Z and Wang J (2024). Biomimetic nanomaterials in myocardial infarction treatment: Harnessing bionic strategies for advanced therapeutics. *Mater Today Bio.,* **25**: 100957.

Zhao L, Zhang H, Li N, Chen J, Xu H, Wang Y and Liang Q (2023). Network pharmacology, a promising approach to reveal the pharmacology mechanism of Chinese medicine formula. *J Ethnopharmacol.,* **309**: 116306.

Zhao Y, Cui R, Du R, Song C, Xie F, Ren L and Li J (2025). Platelet-derived microvesicles mediate cardiomyocyte ferroptosis by transferring ACSL1 during acute myocardial infarction. *Mol biotechnol.,* **67**(2): 790-804.

Zhou Y, Li Y, Yang Z, Zhao L and Wang Y (2025). Discovery of active compounds in Danshen–Chuanxiong formula for blood–brain barrier protection: A multi-parametric study using an OGD/R-induced spheroid model. *J Nat Med.,* **79**(5): 1122-1139.